Nanoscale Advances

ROYAL SOCIETY OF CHEMISTRY

PAPER

View Article Online
View Journal | View Issue

Cite this: *Nanoscale Adv.*, 2022, **4**, 4597

A phosphoric anion layer inhibits electronic current generation and nanotube growth during anodization of titanium

Ziyu Zhao,[a] Shiyi Wang,[a] Jiazheng Zhang,[b] Lin Liu, *[b] Longfei Jiang,[a] Xiangyue Xu[a] and Ye Song*[a]

Received 4th July 2022
Accepted 12th September 2022

DOI: 10.1039/d2na00433j

rsc.li/nanoscale-advances

Nowadays the formation mechanism of anodic TiO_2 nanotubes has attracted extensive attention. Field-assisted dissolution ($TiO_2 + 6F^- + 4H^+ \rightarrow [TiF_6]^{2-} + 2H_2O$) has been considered as the causal link to the formation and growth of nanotubes. But it is hard for this theory to explain three stages of the current–time curve. Here, the anodization of titanium was studied by adding different concentrations of H_3PO_4 (0%, 4 wt%, 6 wt%, 8 wt%, and 10 wt%) in ethylene glycol containing the same concentration of NH_4F (0.5 wt%). The results prove that under the action of the same concentration of NH_4F, the growth rate of nanotubes decreases obviously with the increase of H_3PO_4 concentration, and the second stage of the current–time curve is also prolonged simultaneously. These experimental facts cannot be interpreted by field-assisted dissolution theory and the viscous flow model. Here, an anion layer formed by H_3PO_4 and the electronic current theory are ably used to explain these facts reasonably for the first time.

1. Introduction

In recent years, anodic TiO_2 nanotubes and porous anodic oxides have been widely applied in solar cells, supercapacitors and various sensors.[1–5] However, the formation mechanism of such porous structures and nanotube structures remains highly controversial. Taking the formation mechanism of anodic TiO_2 nanotubes as an example, according to the traditional theory, the field-assisted dissolution reaction ($TiO_2 + 6F^- + 4H^+ \rightarrow [TiF_6]^{2-} + 2H_2O$) involving F^- ions has always been considered as the root cause of the formation and growth of nanotubes.[6–10] Schmuki *et al.*[10] believed that there should be a balance between oxide growth and dissolution during anodization. However, these theories cannot clarify the three stages of the current–time curve during anodization.[11–17] Thompson *et al.*[18] concluded that the above field-assisted dissolution reaction does not contribute to the current variation of anodization. They pointed out that the growth rate of oxide is much higher than the rate of oxide dissolution, and it is impossible to keep a balance between oxide growth and dissolution during anodization.[18] This view is also proved by other groups.[19–22] Moreover, Skeldon *et al.*[21] demonstrated that the dissolution rate of alumina is only about 1 nm min^{-1}, which is much smaller than the growth rate of porous alumina of about 150 nm min^{-1}.[22] Macak *et al.*[6] also demonstrated that the growth rate of anodic TiO_2 nanotubes is much higher than 150 nm min^{-1}. Shen *et al.*[23] also obtained TiO_2 nanotubes in sodium nitrate or potassium nitrate electrolyte without fluoride ions. Thus it can be concluded that the dissolution reaction involving fluoride ions is not the real cause of the formation of TiO_2 nanotubes.

In order to explore the physical significance of the current–time curve during anodization of titanium which proceeds in an electrolyte containing NH_4F and reveals the real cause of the formation of TiO_2 nanotubes, the anodization process of titanium in a mixed electrolyte containing 0.5 wt% NH_4F and different proportions of H_3PO_4 was comparatively studied. The results show that the current–time curves with three stages are obvious in pure NH_4F electrolyte without H_3PO_4, and the growth rate of nanotubes is the fastest. With the increase of H_3PO_4 concentration in electrolyte, three stages of the current–time curve disappear, and the growth rate of nanotubes declines gradually. No nanotubes were even present in EG electrolyte involving 0.5 wt% NH_4F and 10 wt% H_3PO_4. This fact proves that the growth rate of the nanotubes is not directly related to the concentration of F^- ions, whose real role is to cause the generation of electronic current and the release of oxygen gas, while the phosphoric anion layer formed as a hindering layer will prevent the generation of electronic current. To the best of our knowledge, this view has not been reported yet.[1,24,25]

2. Experimental details

2.1 Pretreatment

The anodized substrate was a commercial titanium sheet (purity, 99.99%) with a thickness of 0.2 mm. The whole titanium

[a]Key Laboratory of Soft Chemistry and Functional Materials of Education Ministry, Nanjing University of Science and Technology, Nanjing 210094, China. E-mail: soong_ye@sohu.com

[b]School of Environmental and Chemical Engineering, Jiangsu Ocean University, Lianyungang 222005, China. E-mail: liulin@jou.edu.cn

foil was cut into small sheets of 1 cm × 6 cm, and then the rough cutting edge was polished with sandpaper until smooth. The titanium sheet was picked up with tweezers and immersed in a polishing solution containing HF (40.0%, analytical purity), HNO_3 (66.0%, analytical purity) and deionized water (1 : 1 : 2 by volume) for polishing for 15 seconds. After that, the titanium strips were put into deionized water and rinsed until there was no ion residue on the surface. Then the titanium sheet was removed from the deionized water and dried naturally in air. The titanium sheet was wrapped with insulating tape to ensure that the exposed area of the titanium sheet immersed in the electrolyte is 1 cm × 2 cm on one side (4 cm^2 on both sides).

2.2 Composition of electrolyte

The original electrolyte was an ethylene glycol solution containing 2 wt% water and 0.5 wt% NH_4F. Four electrolytes were obtained by adding 4 wt%, 6 wt%, 8 wt%, and 10 wt% phosphoric acid to the original electrolyte, respectively. These four electrolytes have approximately equal concentrations of NH_4F and unequal concentrations of H_3PO_4. The concentration of phosphoric acid used here was 85 wt%. As a result, the water content of the new four electrolytes configured increased slightly, and the concentration of ammonium fluoride was considered to be essentially unchanged.

2.3 Anodization

The mixed electrolyte was poured into a 50 ml plastic beaker with a titanium sheet as the anode and graphite as the cathode. The anodization temperature was controlled at 20 °C ± 0.1 °C using a thermostat water bath.

The first group of experiments: the titanium was anodized for 600 s at a constant voltage of 50 V in the mixed EG electrolyte with different contents of H_3PO_4 (0 wt%, 4 wt%, 6 wt%, 8 wt%, and 10 wt%), respectively.

The second group of experiments: the titanium was anodized for 600 s at a constant voltage of 60 V in the mixed EG electrolyte with different contents of H_3PO_4 (0 wt%, 4 wt%, 6 wt%, 8 wt%, and 10 wt%), respectively.

The third group of experiments: the titanium was anodized for 600 s at a constant voltage of 70 V in the mixed EG electrolyte with different contents of H_3PO_4 (0 wt%, 4 wt%, 6 wt%, 8 wt%, and 10 wt%), respectively.

The experiments were repeated twice for each group. At the end of each experiment, the power was turned off and the anode titanium sheet was removed from the electrolyte, and then it was rinsed with deionized water until no electrolyte content remained on the surface. After that, the titanium sheet was dried naturally in air and collected for later sample preparation. The current–time curve generated during anodization was recorded using computer software, which should become an important reference material for later morphology characterization. Finally, in order to obtain the cross-sectional morphology of anodic oxides, a small rectangle of the oxides on the titanium sheet was cut and bent into the shape of Ω, which was characterized by FESEM (Zeiss Supra 55).

3. Results and discussion

3.1 Current–time curve of anodization of titanium in pure NH_4F electrolyte

According to the traditional field-assisted dissolution theory, the dissolution reaction of F^- ions leads to the continuous deepening of holes that transform into nanotubes in the end, which is inconsistent with the experimental facts shown in Fig. 1. Fig. 1 shows the cross-sectional morphology and current–time curves of nanotubes obtained through anodization at 70 V, 60 V and 50 V for 10 minutes in 0.5 wt% NH_4F electrolyte. As shown in Fig. 1a, c and e, the lengths of nanotubes are 6.866 μm, 5.147 μm and 2.892 μm, respectively. It can be found that the length of nanotubes is not directly related to the concentration of NH_4F, while the length of nanotubes increases with the rise of anodizing voltage in anodization, whereas the relationship between the length of nanotubes and anodizing voltage is not linear. The fact is that the growth rates of nanotubes are 687 nm min^{-1}, 515 nm min^{-1} and 289 nm min^{-1} at 70 V, 60 V and 50 V separately, indicating that the growth rate of nanotubes becomes faster due to the increase of anodizing voltage. That is to say, the growth rate of nanotubes is not strictly related to the concentration of F^- ions in the electrolyte since the concentration of NH_4F is the same (0.5 wt%) for the three groups. As shown in Fig. 1d and f, when the anodizing voltage is 60 V or 50 V, the current–time curve drops at first and then rises, and finally the anodizing current is steady at the third stage (III). Fig. 1d and f correspond to the stable current density of 20 mA cm^{-2} and 8 mA cm^{-2} at stage III. The traditional theory holds that the reason why the anodizing current of stage III is almost stable is that the field-assisted dissolution of oxide and the growth of oxide reach dynamic equilibrium.[10] Besides, it is also believed that the balance between the growth and dissolution of oxides is the prerequisite for the growth of nanotubes.[10,26–28] However, the current curve in stage III shown in Fig. 1b also kept the trend of rising in stage II, and there was no stable anodizing current in stage III, which fully proves that the stability and instability of anodizing current in stage III were not necessarily related to the balance between oxide growth and dissolution.[19,23] Li *et al.*[11] reported that the growth rate of nanotubes is much higher than the rate of oxide dissolution. The anodizing current in stage III keeps rising, as shown in Fig. 1b, which proves that there is no balance between oxide growth and oxide dissolution during the growth of nanotubes. Also, in terms of the growth rate of nanotubes captured in Fig. 1a, c and e, the balance of the growth and dissolution of oxides is not the prerequisite for the growth of nanotubes. Admittedly, how to explain the changing rule of the current–time curve in Fig. 1b, d and f and the relationship between the length of nanotubes and the growth rate of nanotubes has always been a challenge for metal anodization.[20,28–31]

3.2 Interpretation of three stages of the current–time curve with the double current model

Fig. 2 shows the schematic diagram of nanotube formation depending on the oxygen bubble model during anodization of

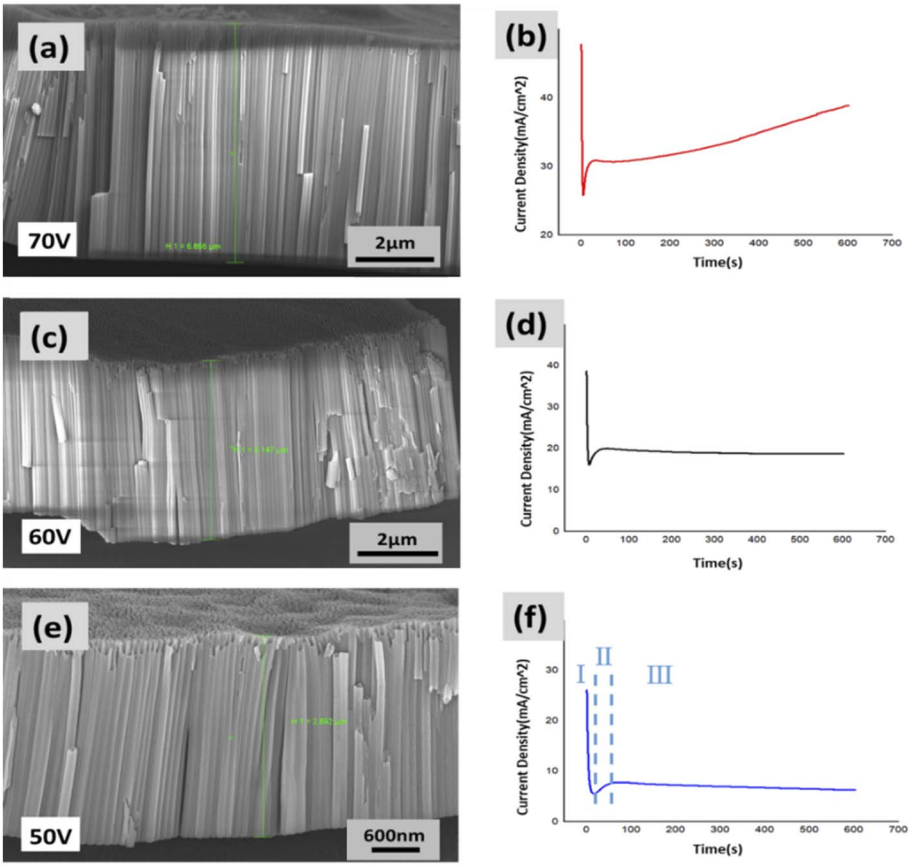

Fig. 1 FESEM images of titanium anodized in the same fluoride-containing EG electrolyte for 600 s (20 °C) at applied voltages of 70 V (a), 60 V (c), and 50 V (e) and the corresponding current–time curves (b, d and f).

titanium.[32–36] We prefer to combine Fig. 2 and 1f to illustrate three stages of the current–time curve and the growth process of nanotubes.[33] In stage I shown in Fig. 1f, the anodizing current decreases rapidly, because in this stage, the total anodizing current is dominated by the ionic current forming oxide. The relation between the ionic current and oxide thickness is as follows:

$$J_{\text{ion}} = A\mathrm{e}^{\beta E} = A\mathrm{e}^{\beta U/d}$$

Here, E represents the electric field intensity, U represents the applied voltage during anodization, d represents the oxide thickness of the barrier oxide layer formed, and A and β are temperature-dependent constants.[33]

Fig. 2a–c describe the process during the first stage with the corresponding current–time curve (Fig. 1f). Fig. 2a shows that at the moment anodization just starts, the electric field (E) approaches its maximum, so the ionic current reaches its peak at the same time, which leads to the rapid growth of anodic oxide. As the thickness of the oxide film increases, the ionic current decreases exponentially. In the first stage of the decline of anodizing current, with the increase of the thickness of the oxide film, an anion contaminated layer is formed at the electrolyte/oxide interface. This kind of layer is mainly generated by anions in the electrolyte (F^-, OH^-, *etc.*) infiltrating into the oxide under the action of the electric field. Also, a new barrier oxide layer is formed at the titanium/oxide interface. With the extension of anodization, the thickness of the anion contaminated layer and barrier oxide layer gradually increase as Fig. 2b and c shown, and also the electric field as well as the ionic current accordingly increase. Diggle *et al.*[37] pointed out that in the anodizing process, the ionic conductance is principal in the case of a high electric field while the electronic conductance is more likely to generate under the situation of a low electric field. Thus, when the anodic oxide grows to a critical thickness, the electric field decreases and the electronic conductance begins to develop. The relation between the electronic current and oxide thickness is as follows:

$$J_{\text{e}} = J_0\mathrm{e}^{\alpha d}$$

Here, d represents the oxide thickness of the barrier oxide layer formed, J_0 is the primary electronic current and α is the impact ionization coefficient.[38] The initial avalanche electronic current is derived from anion discharge at the interface between the contaminated layer and barrier oxide layer as shown in Fig. 2.[39] As a result, anodic TiO_2 nanotubes exhibit a double layer structure in many cases.[39,40]

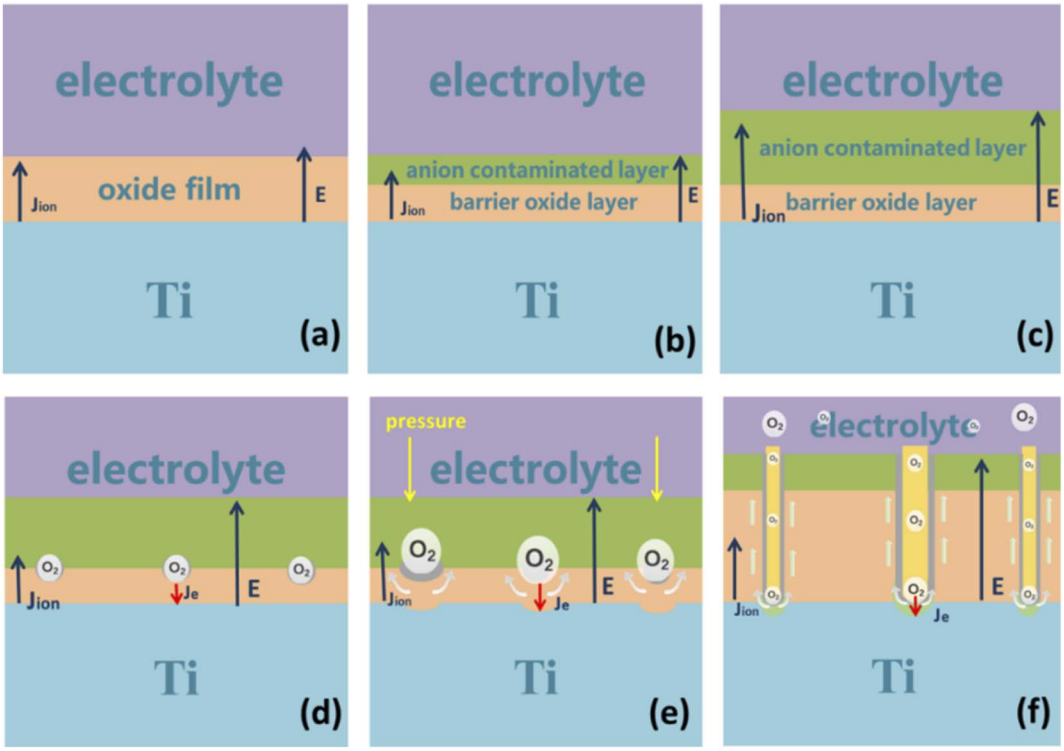

Fig. 2 Schematic diagram of the oxygen bubble model forming nanotubes.

When it comes to the critical thickness corresponding to the lowest point in Fig. 1f, the ionic current reaches the minimum value, while the electronic current develops with the increase of oxide thickness. Therefore, the total anodizing current of the second stage in Fig. 1f increases from the lowest point. Electronic current is caused by anion discharge at the interface between the contaminated layer and the barrier oxide layer.[39] In the anion contaminated layer, both F^- and OH^- can possibly release electrons, but the oxygen gas ($4OH^- = 2H_2O + O_2\uparrow + 4e^-$) is more likely to be produced by OH^- (shown in Fig. 2d and e), since the electronic current and release of oxygen gas also occur in the electrolyte without F^- ions.[23] We believe that during anodization in the electrolyte containing 0.5 wt% NH_4F, F^- ions accumulating on the interface, between the contaminated layer and the barrier oxide layer, are not only helpful for the generation of electronic current but also the release of oxygen gas.[39] This inference will be comprehensively proved in the following anodization with the mixed electrolyte of H_3PO_4 and NH_4F. In Fig. 2e and f, the expansion of oxygen bubbles opens the top contaminated layer, and the electrolyte all enters the bottom of the nanotube. Therefore, the thickness of the barrier layer at the bottom of the nanotube basically remains unchanged, leading to stage III in Fig. 1f, in which the ionic and electronic currents are basically in a stable state. Compared with the voltage of 50 V, when the applied voltage is 70 V, the thickness of the barrier layer is thicker and the electronic current is larger. Therefore, the curve in Fig. 1b keeps an upward trend in stage III, indicating that the electronic current is larger at 70 V and more oxygen bubbles are released, which also leads to a higher growth rate of the nanotubes at 70 V.

3.3 Evolution of current–time curves and nanotube morphology in the mixed electrolyte of NH_4F and H_3PO_4

Fig. 3 shows the FESEM images of the cross-section morphology of TiO_2 nanotubes and the oxide film on the titanium obtained after anodization at a constant voltage of 50 V in a mixed electrolyte of NH_4F and H_3PO_4. Fig. 3f shows that the current–time curve anodized in the electrolyte containing 4 wt% H_3PO_4 also has three stages similar to Fig. 1f, but the stable current density of stage III in Fig. 1f is about 8 mA cm^{-2}. In Fig. 3f, the stabilized current density of stage III is only about 1.8 mA cm^{-2}, and thus the length of nanotubes in Fig. 3a and b varies greatly. As seen from Fig. 3f, with the increasing content of H_3PO_4 in the mixed electrolyte, three stages of the current–time curve in Fig. 1f gradually evolve into two stages. For example, with 6 wt% H_3PO_4, the anodizing current increases very slowly in stage II of the current–time curve. When the concentration of H_3PO_4 reaches 10 wt%, the overall anodizing current in stage II of the current–time curve nearly does not rise, that is to say, there is no electronic current causing the total anodizing current to rise. Therefore, no nanotube embryos are generated in Fig. 3e, yet the corresponding mixed electrolyte contains 0.5 wt% NH_4F. It is sufficient to conclude that the generation of nanotubes is not related to the dissolution reaction of F^- ions, but to the electronic current and the effect of the oxygen bubble model.[23,33,39]

Corresponding to the current–time curves in Fig. 3f, the morphology of nanotubes can be seen clearly from the cross-sectional images in Fig. 3c and d under the condition that the total anodizing current tends to rise due to the appearance of electronic current in stage II. However, as the H_3PO_4

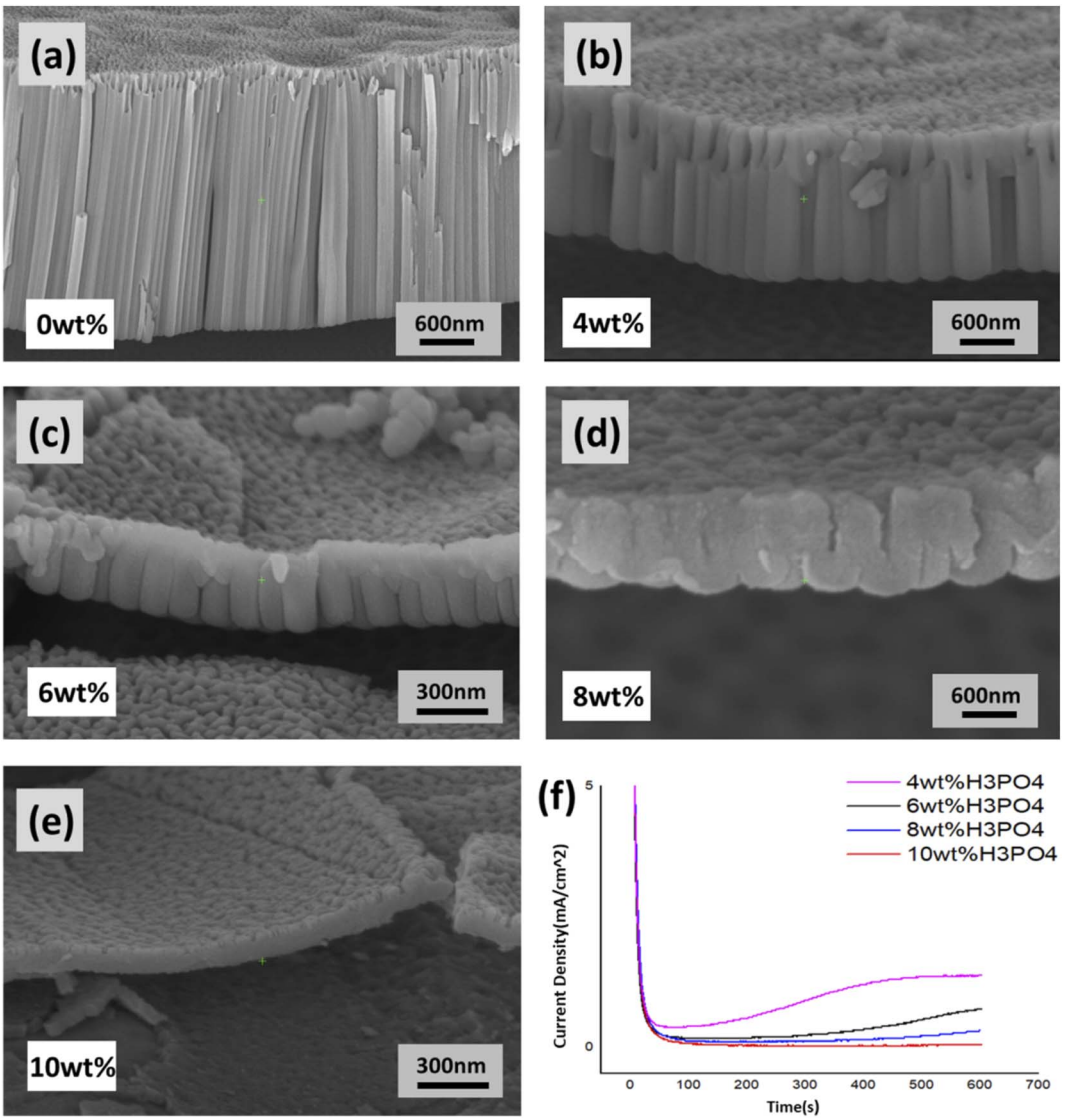

Fig. 3 FESEM images of Ti anodized in the mixed electrolytes with different concentrations of H_3PO_4 (a) 0 wt%, (b) 4 wt%, (c) 6 wt%, (d) 8 wt%, and (e) 10 wt% and corresponding current–time curves (f) obtained at 50 V for 600 s (20 °C).

concentration reaches 10 wt%, no electronic current appears according to the current–time curve, which means that the oxygen bubble model is unable to form any nanotube embryos.[33–35] Therefore, only a section of the dense oxide film can be seen in Fig. 3e. In these electrolytes, the concentration of NH_4F is the same (0.5 wt%), but the concentration of H^+ increases with the rise of H_3PO_4 concentration. Thus the chemical reaction ($TiO_2 + 6F^- + 4H^+ \rightarrow [TiF_6]^{2-} + 2H_2O$) should accelerate the field-assisted dissolution greatly,[24] while the fact of the dense film shown in Fig. 3e proves that the reaction of field-assisted dissolution does not occur at all. The following exposition will further analyze the essential reason why the electronic current disappears with the increase of H_3PO_4 concentration during anodization in the mixed electrolyte of NH_4F and H_3PO_4.

Fig. 4 shows FESEM images of the cross-sectional morphology of TiO_2 nanotubes and titanium oxide films obtained after anodization at a constant voltage of 60 V in the mixed electrolyte of NH_4F (0.5 wt%) and H_3PO_4. Their current–time curves and the morphology of the oxide film are completely similar to that shown in Fig. 3, which further supports the conclusion of Fig. 3.

3.4 Origin of the disappearance of electronic current in a mixed electrolyte containing H_3PO_4 with the same NH_4F concentration (0.5 wt%)

Fig. 5 shows the distribution of anions in the anion contaminated layer close to the electrolyte anodized in the mixed electrolyte of NH_4F and H_3PO_4. On the interface, close to the barrier oxide layer, the first layer is composed of PO_4^{3-} for PO_4^{3-} is a trivalent anion that receives the largest electric field force under the effect of the same electric field. Hence an anion contaminated layer dominated by PO_4^{3-} is formed on the interface near the barrier oxide layer. This phosphoric anion

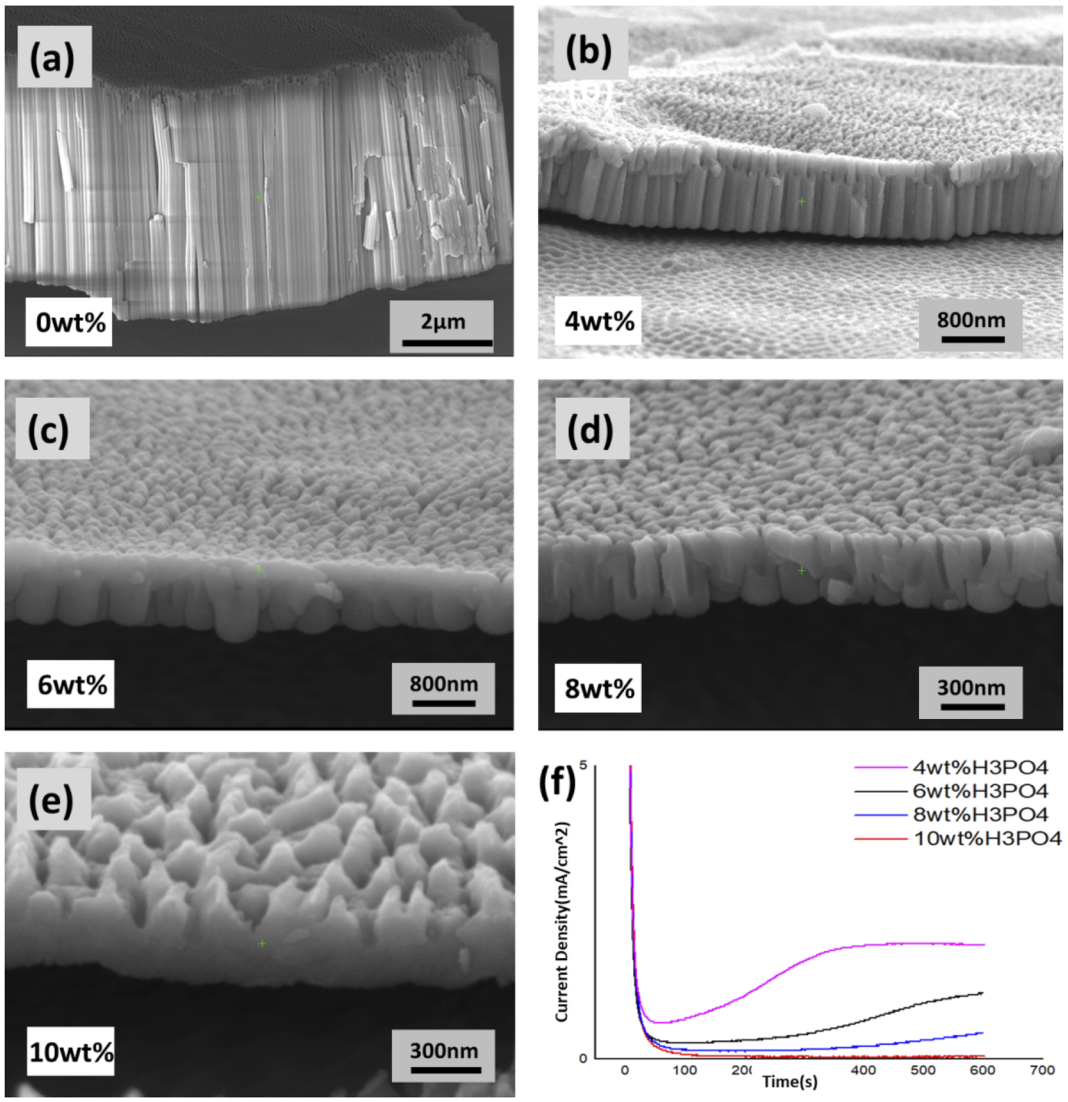

Fig. 4 FESEM images of Ti anodized in the mixing electrolytes with different concentrations of H_3PO_4 (a) 0 wt%, (b) 4 wt%, (c) 6 wt%, (d) 8 wt%, and (e) 10 wt% and the corresponding current–time curves (f) obtained at 60 V for 600 s (20 °C).

layer formed as a hindering layer will prevent the generation of electronic current.

The second layer is occupied by divalent anions of HPO_4^{2-} and O^{2-} which are less likely to lose electrons than OH^- and generate electronic current. The third layer is the anion contaminated layer comprised of monovalent anions farthest from the interface of the barrier oxide layer, including F^- and OH^-. It seems that OH^- and F^- ions are away from the interface of the barrier oxide layer, and thus the electronic current and the probability of oxygen gas release are reduced to a great extent. That is to say, as the concentration of H_3PO_4 increases in the mixed electrolyte, the time used to produce electronic current and release oxygen gas is dramatically extended, which is shown in Fig. 3f and 4f, in which the current–time curves of stage II are distinctly extended. Therefore, when the H_3PO_4 concentration reaches 10 wt%, no electronic current is generated during anodization of 600 s as shown in Fig. 4f, and there are no nanotube embryos formed by oxygen bubbles.[35] However, in pure 0.5 wt% NH_4F electrolyte without H_3PO_4, the time used to generate electronic current is less than 50 seconds (as shown in Fig. 1b, d and f). As there is no anion hindering layer formed by polyvalent anions such as PO_4^{3-} ions and HPO_4^{2-} ions, the anion contaminated layer is only composed of F^- and OH^- ions. As a result, it is easier for OH^- ions to discharge and produce electronic current and oxygen bubbles. Under this effect, the newly formed oxide, in the form of viscous flow, grows up around oxygen bubbles which begin to take shape as nanotube embryos, as shown in Fig. 2e.[29,30,35,41]

3.5 Different surface morphology and formation mechanisms of the oxide film

Fig. 6 shows the surface morphology of the oxide film obtained at different voltages in the electrolyte containing the same concentration of NH_4F (0.5 wt%) and different proportions of H_3PO_4. Fig. 6a and b show the surface morphology of nanotubes

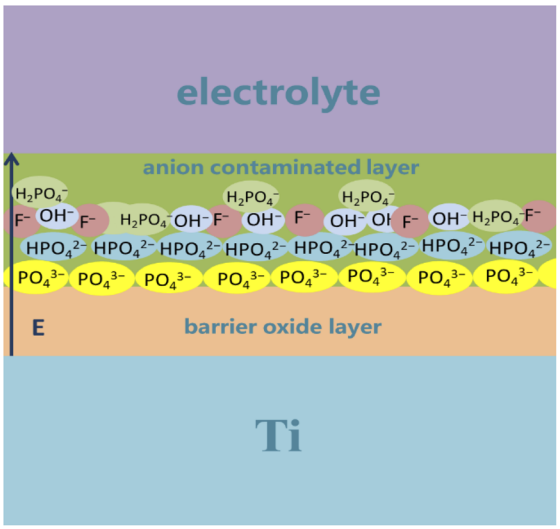

Fig. 5 Distribution of anions in the contaminated layer during anodization in the mixed electrolyte consisting of H_3PO_4 and NH_4F.

obtained by anodization for 600 seconds in the electrolyte only containing 0.5 wt% NH_4F, whose corresponding cross-sectional morphologies are shown in Fig. 3a and 4a. In terms of the surface morphology, the porosity in Fig. 6a is larger than that in Fig. 6b. Also, the inner diameter of holes in Fig. 6a is bigger than that in Fig. 6b. The reason why these phenomena happen is that the electronic current is higher at 60 V, resulting in more oxygen gas release from nanotubes shown in Fig. 6a than in Fig. 6b. The deep holes indicated in Fig. 6a are formed due to the effect of the oxygen bubble model, and these deep holes on the surface correspond to the nanotubes below the surface. Since the images in Fig. 6a and b were obtained in the electrolyte with the same concentration of NH_4F, the difference in surface morphology between Fig. 6a and b does not result from the corrosion of F^- ions, but the difference of electronic currents at different voltages. With more oxygen gas release, the inner diameter of deep holes on the surface becomes larger.

In Fig. 6a, besides deep holes corresponding to nanotubes, shallow holes are also marked. These shallow holes can be found in Fig. 6b. We believe that these shallow holes are different from deep holes. They are shaped by oxygen bubbles that stay on the surface and cannot immediately release from the oxide film. In other words, due to the high electronic current in pure NH_4F electrolyte, oxygen bubbles not only release from the bottom of nanotubes, but also a small amount of them release from the surface of the oxide film. This kind of hole on

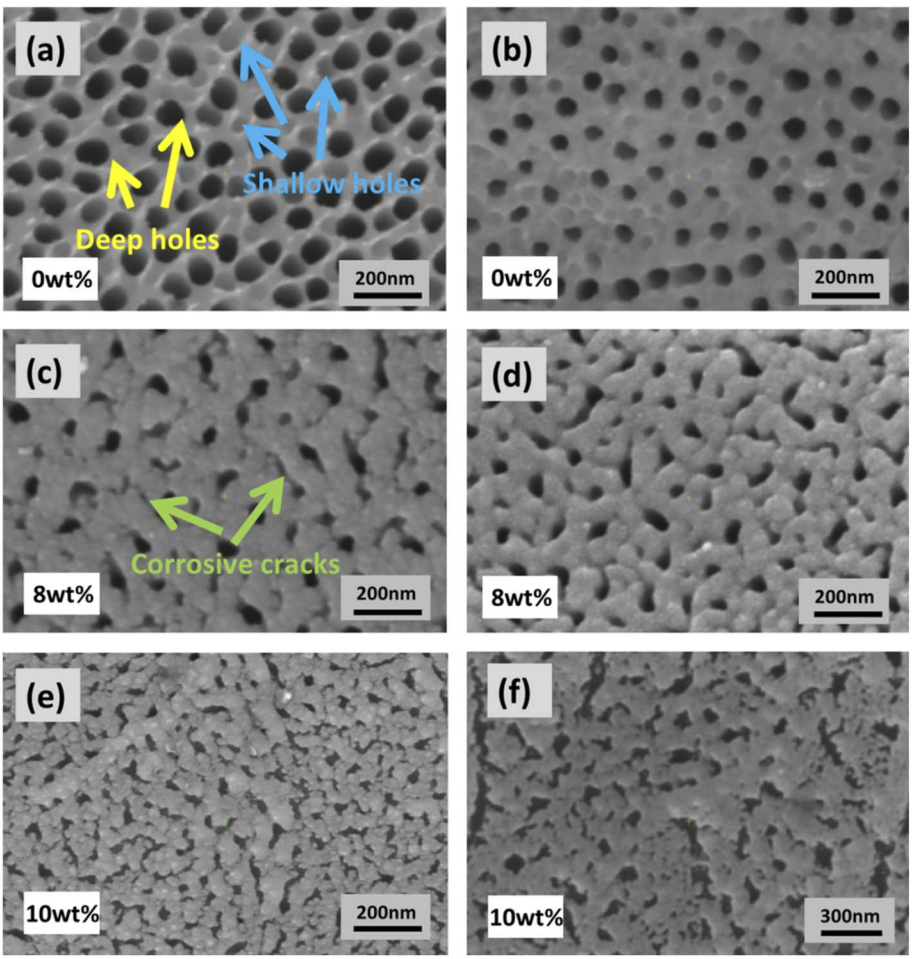

Fig. 6 FESEM images of Ti anodized in different electrolytes (a) and (b) without H_3PO_4 at a voltage of 60 V (a) and 50 V (b), respectively; with 8 wt% H_3PO_4 at a voltage of 50 V (c) and 60 V (d), respectively; with 10 wt% H_3PO_4 at a voltage of 50 V (e) and 70 V (f), respectively.

the surface of the oxide film is mainly shaped by oxygen bubbles on the surface. Because of the pressure of electrolyte and external atmospheric pressure, the oxygen bubbles on the surface cannot release at once. Therefore, the effect of the oxygen bubble model comes into play. The influence of atmospheric pressure on anodization of metals has been demonstrated by researchers.[31,42]

Fig. 6c and d show the surface morphology of the anodic oxide film obtained in an electrolyte consisting of 0.5 wt% NH_4F and 8 wt% H_3PO_4. The numbers of shallow holes and deep holes on the surface in Fig. 6c and d are far lower than those in Fig. 6a and b, which is due to the fact that the production of electronic current and oxygen bubbles in the electrolyte with 8 wt% H_3PO_4 during anodization is much less than that in pure NH_4F electrolyte. Different from Fig. 6a and b, some corrosive cracks are seen on the surface of the oxide film. It is believed that the dissolution reaction of F^- ions in electrolyte contributes to these cracks in Fig. 6c and e. The cracks are also greatly related to the volume expansion and oxide stress during the growth of the oxide film.[43–47] These corrosive cracks are more obvious in Fig. 6e and f since the surface morphology of the anodic oxide film was obtained in an electrolyte consisting of 0.5 wt% NH_4F and 10 wt% H_3PO_4. It is observed that no nanotubes were formed from the cross-sectional view (as Fig. 3e and 4e) because of the absence of electronic current during the anodizing process for 600 s (as Fig. 3f and 4f shows), which restrains the effect of the oxygen bubble model and hence the formation of nanotubes, even though there are many corrosive cracks on the surface, as shown in Fig. 6e and f.

4. Conclusions

In order to further explore the field-assisted dissolution of F^- ions and figure out the physical meaning of the current–time curve in the process of titanium anodization, which is favorable for revealing the real reasons for the formation of TiO_2 nanotubes, we have researched the change rule of the current–time curve of anodization in a pure electrolyte containing 0.5 wt% NH_4F and a mixed electrolyte composed of H_3PO_4 and NH_4F respectively in this paper. The results show that the growth rate of nanotubes decreases obviously with the increase of H_3PO_4 content. As the H_3PO_4 concentration reaches 10 wt%, even though the electrolyte consists of 0.5 wt% NH_4F, there are no TiO_2 nanotubes on the Ti substrate after anodization for 600 seconds. This fully proves that the field-assisted dissolution involving F^- ions is not the main reason for the nanotube formation, however the role of F^- ions is more likely to produce the electronic current in the Ti anodization. During the anodization, which is in the mixed electrolyte of NH_4F and H_3PO_4, the phosphoric anions ionized from H_3PO_4 form an anion layer on the interface of the barrier oxide layer. This hindering layer would prevent F^- and OH^- from discharge and producing electronic current on the interface of the barrier oxide layer. As a result, the oxygen bubble has no chance to play its role in forming nanotube embryos of titanium oxide without oxygen release. This means that, in this case, only the dense film of titanium oxide can be obtained after anodization of titanium. The dissolution reaction involving F^- merely contributes to producing irregular corrosive cracks on the surface of the dense film of titanium oxide.

Author contributions

Ziyu Zhao: methodology, and writing – original draft. Shiyi Wang: methodology, writing – review & editing, and formal analysis. Jiazheng Zhang: writing – review & editing, and investigation. Lin Liu: conceptualization, and project administration. Longfei Jiang: formal analysis. Xiangyue Xu: investigation. Ye Song: supervision.

Conflicts of interest

There are no conflicts to declare.

Acknowledgements

This work was financially supported by the National Natural Science Foundation of China (Grant no. 51777097 and 51577093) and the National Undergraduate Training Program for Innovation and Entrepreneurship (202110288048).

References

1 A. Ruiz-Clavijo, O. Caballero-Calero and M. Martín-González, *Nanoscale*, 2021, **13**, 2227–2265.
2 Z. Y. Yuan, S. W. Zhang, F. L. Meng, H. Zhang and K. Y. Zuo, *IEEE Sens. J.*, 2020, **20**, 4275–4282.
3 S. X. Liu, J. L. Tian, S. Wu, W. Zhang and M. Y. Luo, *Nano Energy*, 2022, **93**, 106812.
4 Y. L. Wang, R. Jin, N. Sojic, D. C. Jiang and H. Y. Chen, *Angew. Chem., Int. Ed.*, 2020, **59**, 10416–10420.
5 L. Bai, Y. Zhao, P. Chen, X. Y. Zhang, X. B. Huang, Z. B. Du, R. Crawford, X. H. Yao, B. Tang, R. Q. Hang and Y. Xiao, *Small*, 2021, **17**, 2006287.
6 M. Alijani, H. Sopha, S. Ng and J. M. Macak, *Electrochim. Acta*, 2021, **376**, 138080.
7 K. Y. Wang, G. H. Liu, N. Hoivik, E. Johannessen and H. Jakobsen, *Chem. Soc. Rev.*, 2014, **43**, 1476–1500.
8 M. Martín-Gonzalez, R. Martinez-Moro, M. H. Aguirre, E. Flores and O. Caballero-Calero, *Electrochim. Acta*, 2020, **330**, 135241.
9 S. Chen, Y. L. Ni, J. P. Zhang, Y. X. Dan, W. C. Zhang, Y. Song and X. Zhu, *Electrochem. Commun.*, 2021, **125**, 106991.
10 P. Roy, S. Berger and P. Schmuki, *Angew. Chem., Int. Ed.*, 2011, **50**, 2904–2939.
11 P. Z. Li, H. Wang, Y. L. Ni, Y. Song, M. Sun, T. L. Gong, C. Y. Li and X. F. Zhu, *Nanoscale Adv.*, 2022, **4**, 582–589.
12 H. Tsuchiya and P. Schmuki, *Nanoscale*, 2020, **12**, 8119–8132.
13 D. Regonini, C. R. Bowen, A. Jaroenworaluck and R. Stevens, *Mater. Sci. Eng. R*, 2013, **74**, 377–406.
14 J. L. Qin, Z. G. Cao, H. Li and Z. X. Su, *Surf. Coat. Tech.*, 2021, **405**, 126661.

15 J. H. Su, Y. T. Yu, Y. Song, X. P. Shen, Y. Chen, R. Q. Lv and X. Zhu, *J. Electrochem. Soc.*, 2022, **169**, 032502.
16 H. A. El-Sayed, C. A. Horwood, A. D. Abhayawardhana and V. I. Birss, *Nanoscale*, 2013, **5**, 1494–1498.
17 Z. Zhang, Q. Q. Liu, M. F. He, F. Tang, Z. R. Ying, H. Q. Xu, Y. Song, J. Zhu and X. Zhu, *J. Electrochem. Soc.*, 2020, **167**, 113501.
18 J. Oh and C. V. Thompson, *Electrochim. Acta*, 2011, **56**, 4044–4051.
19 J. J. Zhang, W. Q. Huang, K. Zhang, D. Z. Li, H. Q. Xu and X. Zhu, *Electrochem. Commun.*, 2019, **100**, 48–51.
20 Q. Zhou, M. Tian, Z. Ying, Y. Dan, F. Tang, J. Zhang, J. Zhu and X. Zhu, *Electrochem. Commun.*, 2020, **111**, 106663.
21 A. Baron-Wiechec, M. G. Burke, T. Hashimoto, H. Liu, P. Skeldon, G. E. Thompson, H. Habakaki, J. J. Ganem and I. C. Vickridge, *Electrochim. Acta*, 2013, **113**, 302–312.
22 M. S. Yu, Y. Chen, C. Li, S. Yan, H. M. Cui, X. F. Zhu and J. S. Kong, *Electrochem. Commun.*, 2018, **87**, 76–80.
23 R. Z. Zhu, C. Y. Li, P. Li, X. P. Shen, J. Chen, Y. Song and X. F. Zhu, *Electrochem. Commun.*, 2021, **129**, 107093.
24 N. J. Suliali, C. M. Mbulanga, W. E. Goosen, R. Betz and J. R. Botha, *Electrochim. Acta*, 2020, **337**, 135791.
25 C. Y. Li, Y. L. Ni, J. J. Gong, Y. Song, T. L. Gong and X. F. Zhu, *Nanoscale Adv.*, 2022, **4**, 322–333.
26 W. Lee and S. J. Park, *Chem. Rev.*, 2014, **114**, 7487–7556.
27 K. R. Hebert, S. Albu, I. Paramasivam and P. Schmuki, *Nat. Mater.*, 2012, **11**, 162–166.
28 Q. Dou, P. Shrotriya, W. F. Li and K. R. Hebert, *Electrochim. Acta*, 2019, **295**, 418–426.
29 D. J. LeClere, A. Velota, P. Skeldon, G. E. Thompson, S. Berger, J. Kunze, P. Schmuki, H. Habazaki and S. Nagata, *J. Electrochem. Soc.*, 2008, **155**, C487–C494.
30 J. E. Houser and K. R. Hebert, *Nat. Mater.*, 2009, **8**, 415–420.
31 J. Zhang, Y. T. Yu, P. J. Fang, L. Liu, H. Y. Yue, J. L. Ou and A. J. Han, *Electrochem. Commun.*, 2021, **129**, 107086.
32 P. Y. Deng, X. D. Bai, X. W. Chen and Q. L. Feng, *J. Electrochem. Soc.*, 2004, **151**, B284–B289.
33 X. F. Zhu, Y. Song, L. Liu, C. Y. Wang, J. Zheng, H. Jia and X. Wang, *Nanotechnology*, 2009, **20**, 475303.
34 S. W. Zhao, J. Xing, H. W. Fan, S. Y. Zhang, D. Li and X. F. Zhu, *J. Electrochem. Soc.*, 2017, **164**, E187–E193.
35 T. L. Gong, C. Y. Li, X. Li, H. Y. Yue, X. Zhu, Z. Y. Zhao, R. Q. Lv and J. W. Zhu, *Nanoscale Adv.*, 2021, **3**, 4659–4668.
36 J. W. Cao, Z. Q. Gao, C. Wang, H. M. Muzammal, W. Q. Wang, Q. Gu, C. Dong, H. T. Ma and Y. P. Wang, *Surf. Coat. Tech.*, 2020, **388**, 125592.
37 J. W. Diggle, T. C. Downie and C. W. Goulding, *Chem. Rev.*, 1969, **69**, 365–405.
38 J. M. Albella, I. Montero and J. M. Martinez-Duart, *Electrochim. Acta*, 1987, **32**, 255–258.
39 M. S. Yu, C. Li, Y. Yang, S. Xu, K. Zhang, H. Cui and X. Zhu, *Electrochem. Commun.*, 2018, **90**, 34–38.
40 M. Motola, H. Sopha, M. Krbal, L. Hromádko, Z. O. Zmrhalová, G. Plesch and J. M. Macak, *Electrochem. Commun.*, 2018, **97**, 1–5.
41 S. J. Garcia-Vergara, P. Skeldon, G. E. Thompson and H. Habazaki, *Electrochim. Acta*, 2006, **52**, 681–687.
42 P. Z. Li, J. Wang, L. Liu, J. Ma, Y. L. Ni, H. Wang and Y. Song, *Electrochem. Commun.*, 2021, **132**, 107146.
43 Ö. Özgür Çapraz, P. Shrotriya, P. Skeldon, G. E. Thompson and K. R. Hebert, *Electrochim. Acta*, 2015, **167**, 404–411.
44 Z. Y. Zhang, Q. Wang, H. Q. Xu, W. C. Zhang, Q. Y. Zhou, H. P. Zeng, J. Yang, J. Zhu and X. F. Zhu, *Electrochem. Commun.*, 2020, **114**, 106717.
45 B. Chong, D. L. Yu, M. Q. Gao, H. W. Fan, C. Yang, W. H. Ma, S. Y. Zhang and X. Zhu, *J. Electrochem. Soc.*, 2015, **162**, H244–H251.
46 D. S. Guan and Y. Wang, *Nanoscale*, 2012, **4**, 2968–2977.
47 F. Riboni, N. T. Nguyen, S. So and P. Schmuki, *Nanoscale Horiz.*, 2016, **1**, 445–466.